# Electronic Supplementary Information

# Gas Phase Condensation of Superparamagnetic Iron Oxide-Silica Nanoparticles – Control of the Intraparticle Phase Distribution

Christian Stötzel, Heinz-Dieter Kurland*, Janet Grabow, Frank A. Müller

Otto Schott Institute of Materials Research, Friedrich Schiller University Jena, 07743 Jena, Germany

**Content:**



## S1 Infrared absorptions of the raw powders hematite and quartz

In order to compare the infrared absorption characteristics of the components of the raw powder mixtures, α-$Fe_2O_3$ and α-quartz, their Fourier transform infrared (FTIR) spectra (FTIR spectrometer Alpha-P with evaluation software Opus, Bruker, Rheinstetten, Germany) were measured (Fig. S1). The spectra reveal that the absorption of α-quartz at the wavelength ($\lambda$ = 10.59 µm) of the $CO_2$ laser radiation exceeds the absorption of α-$Fe_2O_3$. Assuming the same laser vaporization conditions this causes a higher vaporization rate of α-quartz compared with α-$Fe_2O_3$.

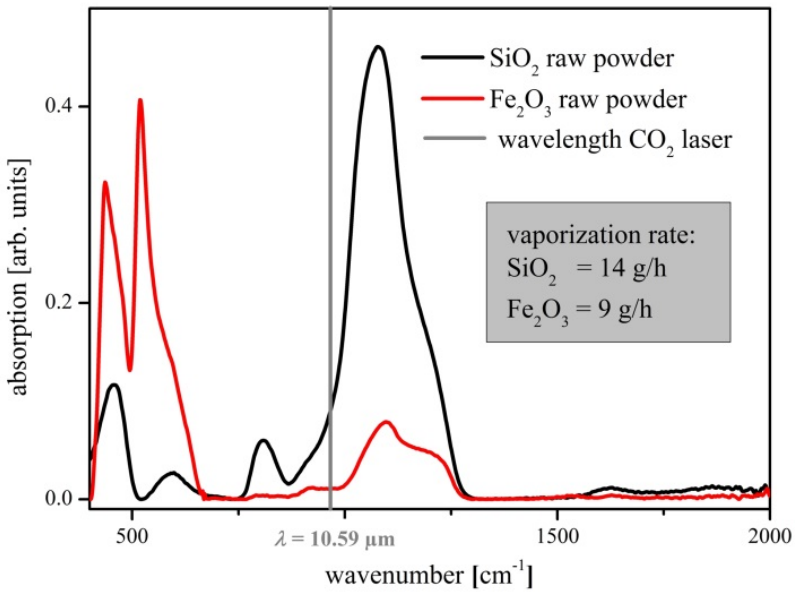


**Fig. S1** Comparison of the infrared absorption characteristics of α-$Fe_2O_3$ (red) and $SiO_2$ (black) at the wavelength ($\lambda$ = 10.59 µm) of the $CO_2$ laser radiation.

## S2 TEM investigation of the spatial distribution of the γ-$Fe_2O_3$ inclusions

TEM micrographs of two composite NPs (sample CN50) with multiple γ-$Fe_2O_3$ segregations were recorded at incrementally (10° increments) altered tilt angles between 0° and 60° (Fig. S2). Segregations located within the volume of the NPs such as no. 6, 10, and 11 as well as segregations at the surface of the NPs such as no. 2, 3, and 13 are strongly displaced upon a tilt. Segregation no. 12 simply changes its position from below to above the projection plane, and segregation no. 9 changes its position only slightly. Given the composite nanoparticle is located within a Cartesian (x-y-z) coordinate system with the z-axis parallel to the incident electron beam, the x-axis as the tilt axis, and the x-y-plane as the projection plane the displacement $d$ for segregations adhering to the surface can be calculated as a function of the tilt angle $\beta$ (Eq. S1).

$$d = \sqrt{2} r_s \sin\left(\frac{180 - \beta}{2} - \sin^{-1}\frac{p}{r_s}\right)\sqrt{1 - \cos\beta} \tag{S1}$$

The parameter $r_s$ is the radius of the cross section perpendicular to the tilt axis at the x-position of the considered segregation and $p$ the distance of the segregation from the tilt axis before the tilting. The calculated displacements for segregations no. 3 and 10 are in good agreement with the measured displacement whereas for segregation no. 9 the actual displacement is far less than predicted. Therefore, segregations no. 3 and 10 must be located close to the composite nanoparticle's surface whereas segregation no. 9 must be located close to the tilt axis.

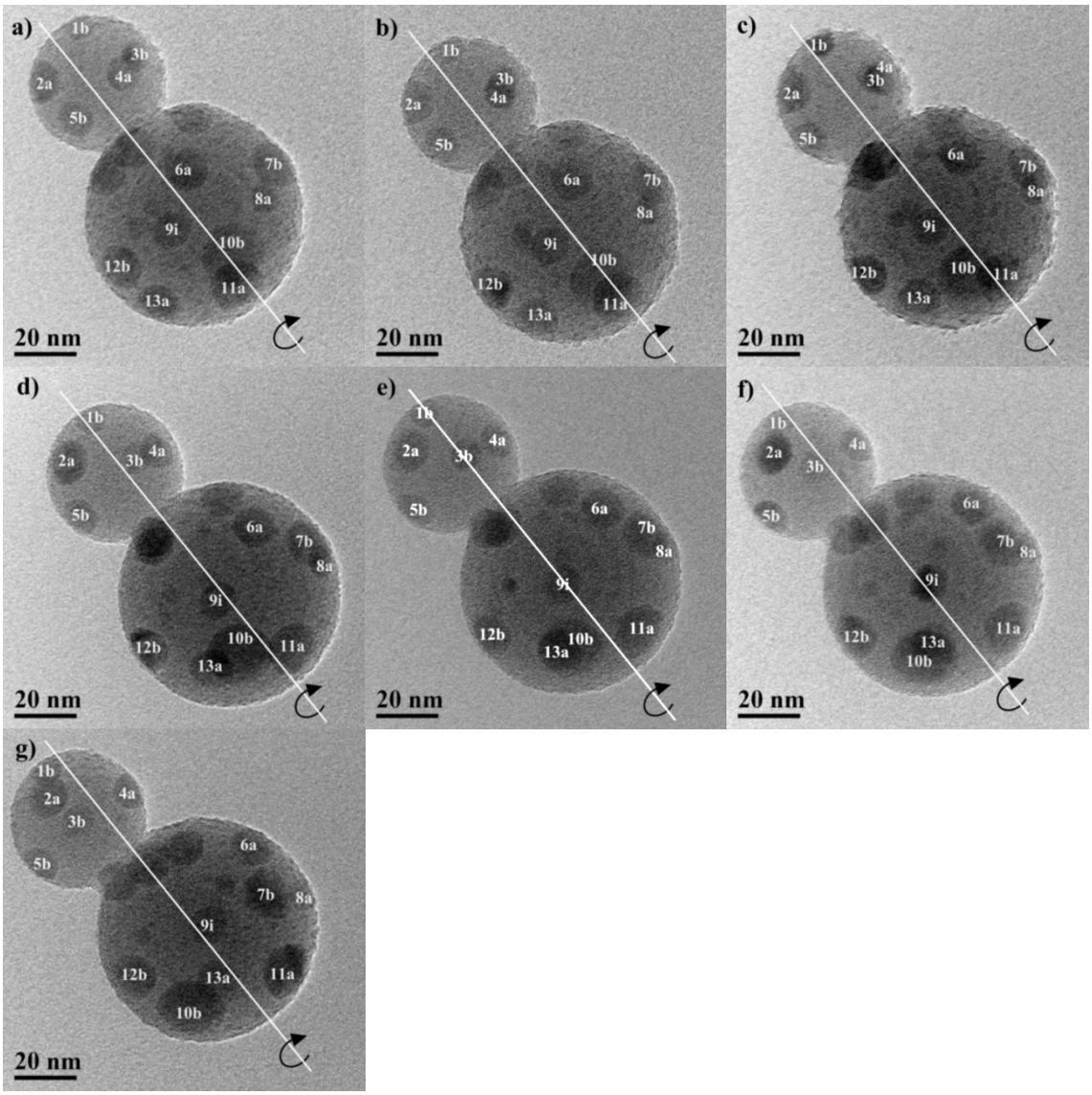


**Fig. S2** Complete series of TEM micrographs of two composite NPs (sample CN50) with multiple γ-$Fe_2O_3$ inclusions recorded at

incrementally (10° increments) altered tilt angles from 0° to 60° (a to g). The segregations are numbered for an easy tracking.

## S3 Particle size distributions of the $Fe_2O_3$@$SiO_2$ nanopowder samples

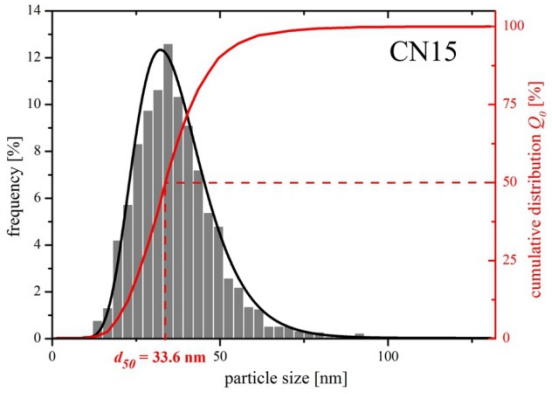


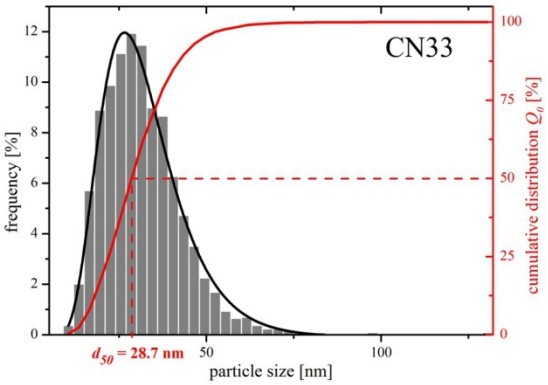


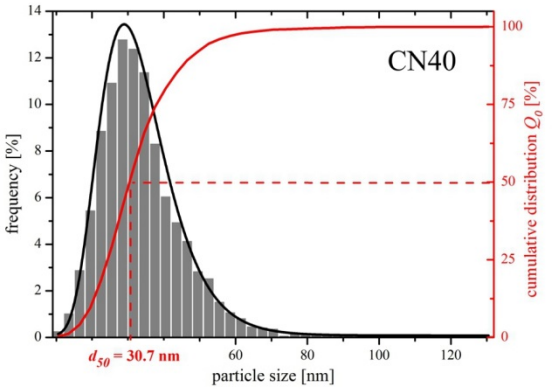


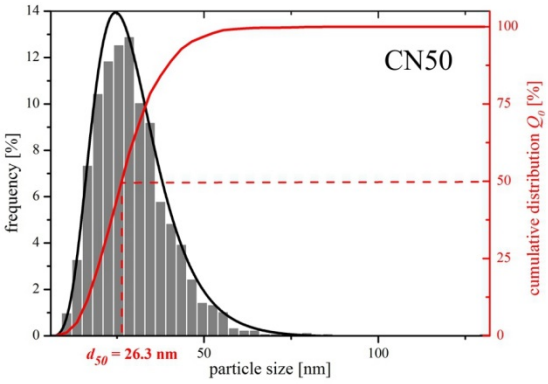


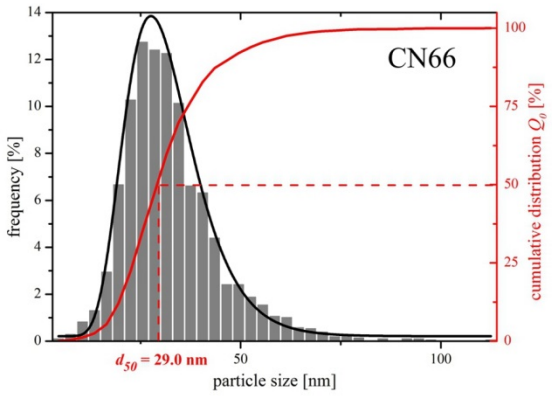


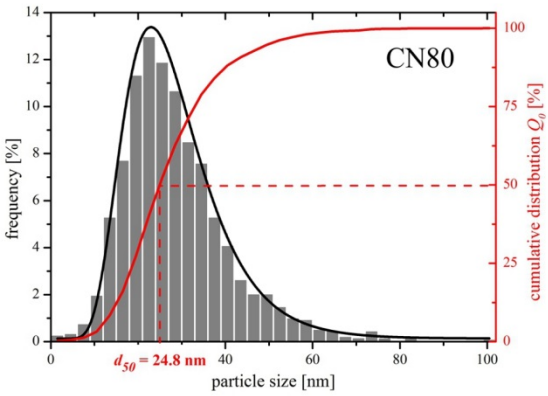


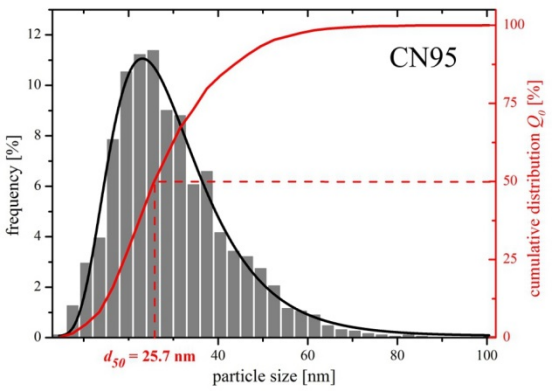

**Fig. S3** Density distributions of the particle diameters on number basis (ordinary $q_0$ and cumulative $Q_0$) and $d_{50}$ diameters of all $Fe_2O_3$@$SiO_2$ nanopowder samples (CN15 to CN95) manually evaluated from TEM micrographs and fitted with log-normal distribution functions.

## S4 ζ-potentials of aqueous dispersions of the composite nanopowders

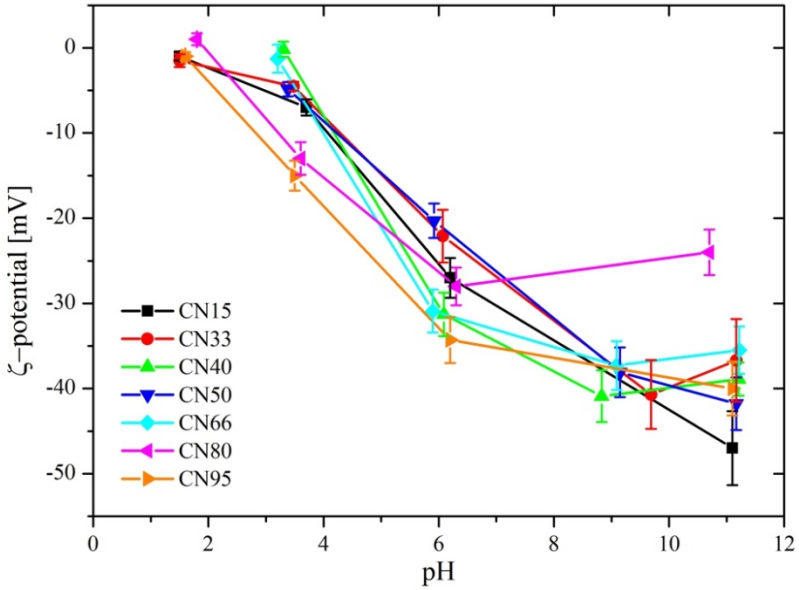


**Fig. S4** ζ-potential of all nanocomposites in aqueous dispersion in the pH range of 2-11.

## S6 Silanization of $Fe_2O_3$@$SiO_2$ composite nanopowders with [3-(2,3-epoxypropoxy)-propyl]-trimethoxysilane

Surfaces activated with epoxy groups are attractive systems for the covalent immobilization of biomolecules. Even at mild conditions epoxides are reactive to many nucleophiles (e.g. hydroxide, amine, or thiol groups) of proteins, and the resulting chemical bonds are very stable. Therefore, the silanization with an epoxysilane can provide a chemically reactive interface for the covalent protein immobilization.[S1]

Thus, in order to prove the reactivity of the particles' silica surface, $Fe_2O_3$@$SiO_2$ composite NPs were silanized with [3-(2,3-epoxypropoxy)-propyl]-trimethoxysilane. In the presence of water the epoxysilane's alkoxy groups are hydrolyzed. Condensation of the silanol groups of the hydrolyzed epoxysilane and silanol groups bonded to the silica surface results in the formation of covalent -Si-O-Si- bridges (Fig. S5). The resulting terminal epoxide group can then be used for further reactions, such as protein immobilization.[S2]

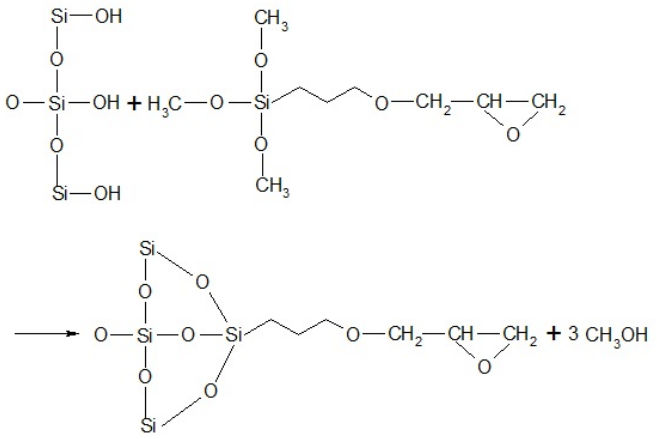


**Fig. S5** Schematic of the reaction of silanol groups on a silica surface with [3-(2,3-epoxypropoxy)-propyl]-trimethoxysilane.

600 mg portions of the $Fe_2O_3$@$SiO_2$ powder samples CN40 and CN80 as well as of the pure $SiO_2$ and γ-$Fe_2O_3$ nanopowders were

weighed into centrifuge tubes. Each sample was dispersed in 0.5 ml [3-(2,3-epoxypropoxy)-propyl]-trimethoxysilane (GLYMO, Merck, Darmstadt, Germany) with 49.5 ml water-free toluene at room temperature. After 18 h the nanopowders were centrifuged and rinsed three times with toluene at 3000 rpm $min^{-1}$ for 2.5 min. Subsequently the rinsed powders were dried at 70°C for 24 h in a drying oven. For comparison, pure γ-$Fe_2O_3$ and $SiO_2$ nanopowders were subjected to the same silanization procedure. Furthermore, blank tests were conducted. For this purpose, CN40 and CN80 nanopowders as well as the γ-$Fe_2O_3$ nanopowder were subjected to the silanization procedure described above. However, the volume of epoxysilane was replaced by toluene.

The chemical bonding of the epoxysilane was qualitatively examined by Fourier transform infrared (FTIR) spectroscopy (FTIR spectrometer Alpha-P with evaluation software Opus, Bruker, Rheinstetten, Germany). The FTIR spectra were recorded (range: 375 $cm^{-1}$ – 4000 $cm^{-1}$, resolution: 2 $cm^{-1}$, number of scans: 100) in attenuated total reflection (ATR) mode. The mass fractions of carbon and hydrogen in the silanized nanopowders were determined by elemental (CHN) analyses (CHN-932 equipped with autosampler and thermal conductivity detector, LECO Instrumente GmbH, Germany). From the carbon and hydrogen portions and the initial masses (2 mg – 3 mg) of the samples the mean molar concentrations $c_{epoxysilane}$ of epoxysilane in the samples were calculated. Furthermore, the NPs' loading densities $\alpha$ with epoxysilane were determined using the molar concentrations $c_{epoxysilane}$ and the measured specific surface areas $S_{BET}$ (cf. Table 1) of the nanopowder samples CN40 and CN80.

In the FTIR spectra (Fig. S6) of the epoxy-silanized $SiO_2$ and $Fe_2O_3$@$SiO_2$ nanopowders the bonding of the epoxysilane to the silica surface of the NPs is indicated by the presence of C–$H_2$ vibrations in the wave number region between 2800 $cm^{-1}$ and 2900 $cm^{-1}$ (Fig. S6, inset). In contrast, these vibrations are missing in the spectrum of the unmodified $Fe_2O_3$@$SiO_2$ nanopowder.

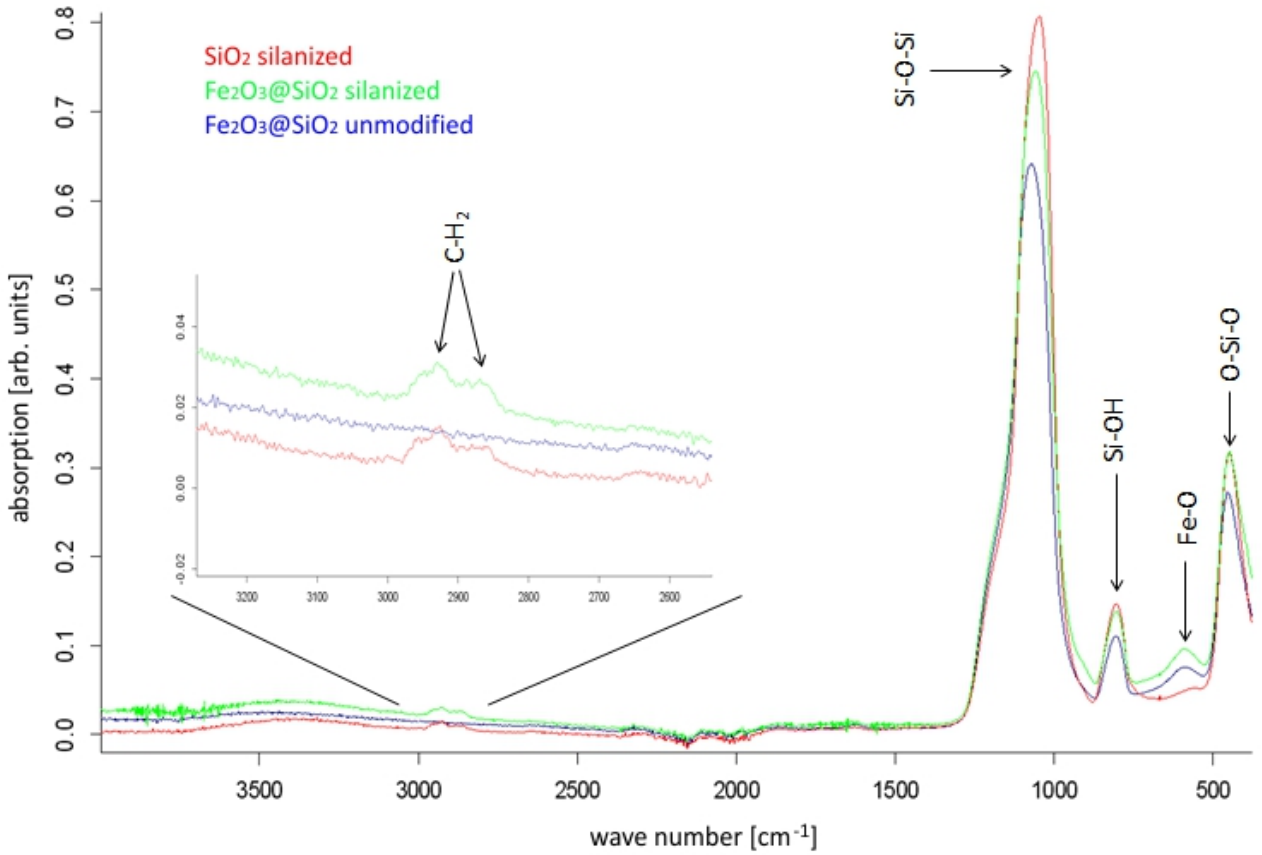


**Fig. S6** FTIR spectra of the epoxy-silanized $Fe_2O_3$@$SiO_2$ (CN80) and $SiO_2$ nanopowders as well as of the unmodified $Fe_2O_3$@$SiO_2$ nanopowder (CN80).

The results of the CHN analysis of the silanized composite nanopowders CN40 and CN80 along with the calculated values of the epoxysilane concentrations in these samples and the NPs' loading densities with expoxysilane are summarized in Table S1.

**Table S1** C and H mass fractions in the silanized nanopowders CN40 and CN80, calculated concentrations $c_{epoxysilane}$ of epoxysilane in these nanopowders, and the NPs' loading densities $\alpha$ with epoxysilane.

| sample | C [mass%] | H [mass%] | $c_{epoxysilane}$ [mol $g^{-1}$] | $\alpha$ [$nm^{-2}$] |
|---|---|---|---|---|
| CN40 | 2.27 | 0.49 | $3.15 \cdot 10^{-4}$ | 2.70 |
| CN80 | 1.71 | 0.32 | $2.37 \cdot 10^{-4}$ | 2.51 |

FTIR spectroscopy (Fig. S6) and CHN analyses (Table S1) confirm the successful silanization of the composite nanopowders CN40 and CN80. In contrast, the CHN analyses of the silanized γ-$Fe_2O_3$ nanopowders as well as of the blank samples resulted epoxysilane concentrations and loading densities with expoxysilane of about $c_{epoxysilane} \approx 0.6 \cdot 10^{-4}$ mol $g^{-1}$ and about $\alpha \approx 1.2$ $nm^{-2}$, respectively. These at least for the blank samples fictitious values apparently reveal the sensitivity limit of the analysis technique.

The silanization of the nanopowders was conducted in water-free epoxysilane/toluene reaction media. However, the reaction of epoxysilane with the NPs' surfaces should not proceed in the absence of water.[S3] The nevertheless successful silanization of the $Fe_2O_3$@$SiO_2$ NPs is attributed to traces of water on their surfaces. These initiate the hydrolysis and condensation of the silane to the NPs' silica surfaces.[S4] Hence, in water-free reaction media the coverage with expoxysilane cannot exceed a monolayer. This is supported by the NPs' loading densities in samples CN40 and CN80 (cf. Table 1) which are below the corresponding loading density $\alpha$ = 4 $nm^2$ [S4] of a closed monolayer of epoxysilane.

**Multimedia file:** Rotating Fe2O3@SiO2 NP.AVI

**Title:** Animated tilting of γ-$Fe_2O_3$@$SiO_2$ nanoparticles with multiple iron oxide inclusions.

**Legend:** The animation illustrates the spatial distribution of γ-$Fe_2O_3$ inclusions within the composite nanoparticles of sample CN 50. It is composed of TEM micrographs of two particles recorded at incrementally altered tilt angles.

**Keywords:** nanocomposite, iron oxide, silica, morphology, spatial distribution, TEM, rotation


S1 Q. Zhang, R.F. Huang and L.H. Guo, *Chinese Sci. Bull.* 2009, **54**, 2620.

S2 Y. Lü, G. Lu, Y. Wang, Y. Guo, Y. Guo, Z. Zhang, Y. Wang and X. Liu, *Adv. Funct. Mater.* 2007, **17**, 2160.

S3 P. Van Der Voort and E.F. Vasant, *J. Liq. Chromatogr. R. T.* 1996, **19**, 2723.

S4 I. Luzinov, D. Julthongpiput, A. Liebmann-Vinson, T. Cregger, M.D. Foster and V.V. Tsukruk, *Langmuir* 2000, **16**, 504.